Spin-wave localization in tangentially magnetized films

Elena V. Tartakovskaya*
Institute of Magnetism NAS of Ukraine, Vernadsky Blvd. 36b, 03142 Kiev, Ukraine
and Institute of High Technologies, Taras Shevchenko National University of Kiev, 03022 Kiev, Ukraine

Martha Pardavi-Horvath
School of Engineering and Applied Science, The George Washington University, Washington, D.C. 20052, USA

Robert D. McMichael†
Center for Nanoscale Science and Technology, National Institute of Standards and Technology, Gaithersburg, Maryland 20899, USA
(Received 13 April 2016; published 28 June 2016)

We present an analytical description of localized spin-wave modes that form in a parabolic field minimum in a thin ferromagnetic film. Mode profiles proportional to Hermite functions are eigenfuctions of the applied field and exchange parts of the equations of motion, and also provide a basis for numerical approximation of magnetostatic interactions. We find that the spin-wave modes are roughly equally spaced in frequency and have roughly equal coupling to a uniform driving field. The calculated mode frequencies and corresponding profiles of localized spin-wave modes are in good agreement with micromagnetic modeling and previously published experimental results on multiple resonances from a series of localized modes detected by ferromagnetic resonance force microscopy.

DOI: 10.1103/PhysRevB.93.214436

I. INTRODUCTION

During the last decade, localization of magnetic excitations (i.e., localization of spin waves) has drawn the attention of many researchers. Localized spin excitations are important for a range of applications from local measurements of magnetic properties to the switching dynamics of novel memory devices and the dynamics of spin torque oscillators.

The mechanism of spin-wave localization can have a variety of physical origins. At the most basic level, excitations are confined to the volume of a magnetic structure [1,2]. In a sheet film, however, spin-wave localization may occur in regions of low effective field, meaning regions where the precession frequency is lower than the range of propagating spin-wave frequencies in the surrounding medium. Without a separation in frequency between localized and propagating modes, a locally prepared excitation would likely couple to propagating waves having the same frequency, allowing the precession energy to disperse. Regions of low effective field occur as a result of material property fluctuations in inhomogeneous materials, and it has been shown through modeling that such localization contributes to broadening of the ferromagnetic resonance linewidth [3].

A fairly common situation where the conditions for spin-wave localization are met occurs in patterned film structures where internal fields may be strongly inhomogeneous, especially near film edges. Localized spin waves have been observed near the edges of ferromagnetic stripes and rectangular elements [4–8], and these edge modes have been used to characterize the effects of lithography [9], oxidation [10], and interactions in multilayer stripe arrays [11]. In straight stripes, the localized spin waves are localized in two dimensions, but remain extended along the film edge, but along a curved film edge, i.e., in ferromagnetic nanodisks, the spin waves can be localized in three dimensions, allowing probes of edge geometry and conditions along sample edges [12,13].

In addition to linear excitations, a rich variety of nonlinear localization phenomena has been explored including propagating solitons and stationary nonlinear excitations such as bullets [14–16] and droplets [17–19] which are self-localized via the intrinsic nonlinearity of the Landau-Lifshitz equations of motion [20].

In this paper, we address small-angle spin-wave modes that are localized in unpatterned films, and we treat a conceptually simple case, in which the magnitude of the local field has a parabolic minimum in the plane of the film. The parabolic field well provides a useful approximation to the stray field of the tip in magnetic scanned-probe experiments, for example, where a magnetized tip can produce significant stray fields. Both calculations and measurements have demonstrated spin-wave localization under such a tip for perpendicular [21–25], tilted [26], and in-plane orientations [13]. Localized spin waves of this type can then be used as probes of material inhomogeneity with spatial resolution similar to the size of the localized mode [13,21]. Additionally, localized spin waves have been used in the "magnetic well" method to nondestructively probe losses in extended films with low damping [27].

This paper is organized as follows. In Sec. II we develop the theoretical basis for analysis of spin waves that are localized in a parabolic field well. In Sec. III we use this analysis to approximate the modes formed in the field minimum due to a magnetic cantilever tip, and we compare the results with micromagnetic calculations. For better quantitative agreement between theory and micromagnetic calculations, we extend the theory to accommodate the case of strongly hybridized modes in Sec. IV. In Sec. V we conclude with a discussion of results in the context of existing models of spin-wave localization in thin films and nanostructures.

*olena.tartakivska@gmail.com
†rmcmichael@nist.gov

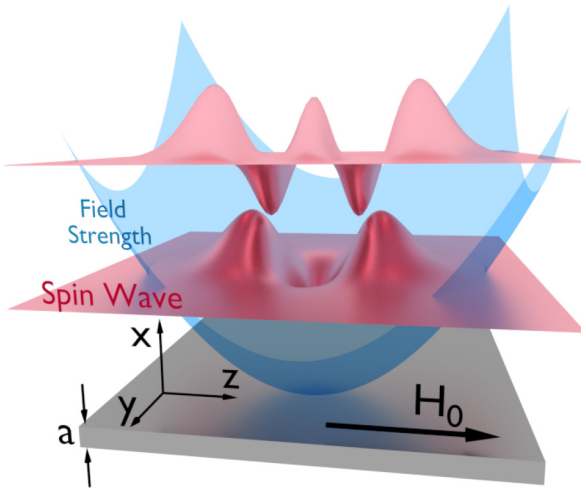

FIG. 1. Schematic representation of localized spin-wave mode profiles formed in a film of thickness a, magnetized in plane. The field is in the z direction while the magnitude of the field has a parabolic spatial dependence.

II. DESCRIPTION OF THE MODEL

Figure 1 conceptually illustrates the situation for an in-plane magnetized film. A magnetic film of thickness a lies in the y-z plane with the x direction along the film normal. An external source creates a field that varies in magnitude over position but is always aligned along the z axis. We create a simple field minimum by allowing the field magnitude to vary in the plane of the film as a parabolic well,

$$H_i(y,z) \approx H_0(1 - C_0 + C_z z^2 + C_y y^2). \tag{1}$$

Here, the internal field H_i includes a uniform applied field H_0 and a parabolic field well with depth H_0C_0 and curvature parameters H_0C_y and H_0C_z. We choose the parabolic field components to be proportional to the applied field in order to treat the case of a field well due to a nearby, partially magnetized sphere. A parabolic magnetic field profile has a number of intrinsic problems, including large field amplitudes far away from the origin and violations of Maxwell's equations. These difficulties serve as reminders that the solutions to this problem are only approximate solutions to any real physical problem.

We treat the magnetization of the film as the sum of the saturation magnetization $\mathbf{M}_0$ and a weakly excited component, $\mathbf{m}(\mathbf{r})$; $\mathbf{M} = \mathbf{M}_0 + \mathbf{m}(\mathbf{r})\exp(i\Omega t)$, and we assume that the static average magnetization $\mathbf{M}_0$ is parallel to the z axis.

An analytic solution for symmetric parabolic field wells (i.e., $C_y = C_z$) has been used to describe spin-wave modes localized by the dipole field from a probe magnet [25,27]. This model was developed for the case of sufficiently small wave vectors, where the exchange fields are negligible. Bessel functions were used to approximate mode profiles and the results are reasonable for the lowest mode of spin-wave spectrum [23]. Here, we treat the case of asymmetric field wells ($C_y \neq C_z$) and we incorporate the exchange interactions explicitly.

To find the frequencies Ω as well as corresponding profiles of spin-wave modes that are localized in the film in the inhomogeneous field we use the Landau-Lifshitz equation of motion. We include the dynamic dipolar field that is generated by the precession of the magnetization of the film, $\mathbf{h} = -\nabla\Phi_M$, and the static parabolic external field.

$$i\frac{\Omega}{\gamma\mu_0}m_x = H_i m_y, - M_0(D\Delta m_y + h_y), \tag{2a}$$

$$-i\frac{\Omega}{\gamma\mu_0}m_y = H_i m_x, - M_0(D\Delta m_x + h_x), \tag{2b}$$

where $M_0 = |\mathbf{M}_0|$ is the saturation magnetization of the film, $\gamma/2\pi = 29.6$ GHz/T is the gyromagnetic ratio, $D = 2A/\mu_0 M_0^2$ is the exchange length squared, and A is the exchange stiffness. The components of the dynamic dipolar field, denoted in Eq. (2) as h_x and h_y, can be expressed as

$$h_u = -\frac{\partial}{\partial u}\int d\mathbf{r}'(\mathbf{m}\cdot\nabla')\frac{1}{|\mathbf{r}-\mathbf{r}'|}. \tag{3}$$

Using the parabolic field given by (1), the equations of motion can be rewritten in terms of a nonlinear differential operator $\Xi(u) = (-\frac{\partial^2}{\partial u^2} + u^2)$ which captures the exchange interactions and the parabolic field:

$$i\frac{\Omega}{\gamma\mu_0}m_x = M_0 D m_y\left[K_z^2\Xi(\xi) + K_y^2\Xi(\eta)\right] + H_0(1-C_0)m_y - M_0 h_y, \tag{4a}$$

$$-i\frac{\Omega}{\gamma\mu_0}m_y = M_0 D m_x\left[K_z^2\Xi(\xi) + K_y^2\Xi(\eta)\right] + H_0(1-C_0)m_x - M_0 h_x. \tag{4b}$$

Here we have also introduced dimensionless coordinates, $\xi = K_z z$, $\eta = K_y y$ with

$$K_z = \left[\frac{H_0 C_z}{M_0 D}\right]^{1/4} \quad \text{and} \quad K_y = \left[\frac{H_0 C_y}{M_0 D}\right]^{1/4}. \tag{5}$$

These K values have dimensions of 1/length, they characterize length scales associated with the well shape and exchange interactions, and they play roles similar to wave numbers.

The differential operator Ξ appears in pairs set off by square brackets in (4). This operator is identical to the Schrödinger equation of the quantum harmonic oscillator with exchange and Zeeman energies taking the place of kinetic and potential energies, respectively. Eigenfunctions $\psi_n(x)$ satisfying $\Xi(x)\psi_n(x) = \lambda_n\psi_n(x)$ are known to be proportional to Hermite polynomials $H_n(x)$ and have the form

$$\psi_n(x) = \frac{1}{\sqrt{2^n n!\sqrt{\pi}}}\exp(-x^2/2)H_n(x), \tag{6}$$

where

$$H_n(x) = (-1)^n\exp(x^2)\frac{d^n}{dx^n}\exp(-x^2), \tag{7}$$

and the normalization condition is

$$\langle\psi_i(x)\psi_j(x)\rangle = \delta_{ij}. \tag{8}$$

We refer loosely to these eigenfunctions as Hermite functions in this paper. The eigenvalues corresponding to the functions $\psi_n(x)$ are $\lambda_n = 2n + 1$.

It is natural to assume that the spatial profiles of the magnetic excitations have a form of products

$$m(y,z) \sim \varphi_{mn}(\eta,\xi) = \psi_m(\eta)\psi_n(\xi). \tag{9}$$

If the dipolar terms, h_x and h_y in (2) and (4), were neglected, the set of orthogonal functions $\varphi_{mn}(\eta,\xi)$ would provide exact solutions for the eigenmodes of the equations of motion. In such a case, modes with different indices would not interact with each other. However, the solution proposed in (9) is not an eigenfunction of the dipolar operator [Eq. (3)], so the presence of the dynamic dipolar fields h_x,h_y leads to an interaction between modes, and much of the remainder of this paper will be concerned with approximating the magnetostatic interactions.

The simplest approach is to use a diagonal approximation [28,29]. Essentially, the approximation assumes that characteristic exchange/well frequency spacing $\gamma M_0 D K^2$ [see (10), below] is strong compared to a characteristic frequency due to magnetostatic effects, $\gamma M_0 K a$, or $\epsilon \equiv a/(DK_i) \ll 1$. Qualitatively, the diagonal approximation will be valid for ultrathin films and "narrow" field wells, i.e., large values of C_y and C_z. We will find below that these conditions are not met for the present example, but the diagonal approximation is a useful first step, nonetheless.

The diagonal approximation leads to the spectra in a simple diagonal form, which corresponds to an allowed set of localized standing modes with frequencies given by

$$\Omega_{mn} = \gamma\mu_0\sqrt{\left(\Omega^0_{mn} - \langle h_y\rangle_{mn}\right)\left(\Omega^0_{mn} - \langle h_x\rangle_{mn}\right)}, \tag{10}$$

where

$$\Omega^0_{mn} = M_0 D\left[K_z^2(2n+1) + K_y^2(2m+1)\right] + H_0(1-C_0). \tag{11}$$

The diagonal matrix elements of the dipole-dipole interaction are calculated by the formula

$$\langle h_i\rangle_{mn} = -\frac{M_0 K_y K_z}{4\pi a}\int d\mathbf{r}\int d\mathbf{r}'\varphi_{mn}(\eta,\xi,)\varphi_{mn}(\eta',\xi') \times \frac{\partial}{\partial i}\frac{\partial}{\partial i'}\frac{1}{|\mathbf{r}-\mathbf{r}'|}, \tag{12}$$

where i can be x or y. These are essentially demagnetization fields in the film-normal and in-plane directions. The sixfold integral can be simplified substantially, and we refer the reader to Appendix A for details of the simplification and tabulated coefficients for expansion in small values of $K_i a$.

III. SPIN WAVES LOCALIZED BY A MAGNETIZED PROBE TIP

In this section we test the present theory with the diagonal approximation, comparing it to micromagnetic solutions for spin waves in a parabolic well. We choose a parabolic well that approximates the potential well created by the probe tip in a recent set of experiments. The tip is a magnetically soft unsaturated sphere of radius R; the distance from the closest point of the tip to the surface of the ferromagnetic thin film is d, while the thickness of the film is a (see Fig. 2). Previous micromagnetic solutions for the full dipolar tip field and the corresponding experiment are described in Ref. [30].

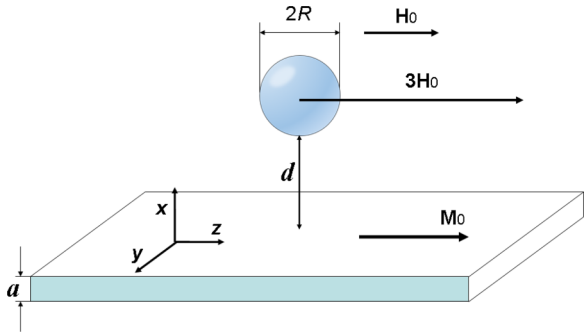

FIG. 2. Geometry of the model, simulating a ferromagnetic resonance force microscopy experiment. The parameters used in calculations are as follows: tip radius, $R = 500$ nm; distance between the tip and the surface of the film, $d = 100$ nm; thickness of the film, $a = 20$ nm.

The magnetic potential at point $\mathbf{r} = (x,y,z)$ is equal to

$$\Phi_0^{\text{sphere}} = \frac{1}{3}M_{\text{sphere}}\frac{R^3 z}{r^3}, \tag{13}$$

and if the value of the applied field is below saturation, $M_{\text{sphere}} = 3H_0$. Here, $r = |\mathbf{r}| > R$ where $\mathbf{r}$ is a radial vector from the center of the sphere to the point. For the thin film, H_i can be written as a function of the two in-plane coordinates, y and z, $H_i \approx H_0 f(y,z)$, where

$$f(y,z) = 1 - \frac{1}{\tilde{r}(y,z)^3}\left(1 - \frac{3(z/R)^2}{\tilde{r}(y,z)^2}\right); \qquad \tilde{r}(y,z) = \sqrt{(R+d+a/2)^2 + y^2 + z^2}/R, \tag{14}$$

To apply the analysis from the preceding section, we make the approximation that the equilibrium magnetization lies parallel to the z axis, i.e., $\mathbf{M}_0 = (0,0,M_0)$, and that the excitations have only two components, $\mathbf{m}(\mathbf{r}) = (m_x,m_y,0)$. In the full description, $\mathbf{H}^{\text{sphere}}$ has three spatial components, and for rigorous analysis, one should take into account deflections of the static magnetization by the x and y components of the dipole field. However, the micromagnetic calculations reveal that the angular deviations of $\mathbf{M}_0$ from the z direction are not dramatic, and in fact the fields from the partially magnetized probe tip are significantly smaller than the applied field H_0.

To apply our model, we approximate the dipole field from the tip with a truncated parabolic field well as illustrated in Fig. 3, where the truncated parabola has the form given by Eq. (1) when $H_i(y,z) < H_0$ and a constant value H_0 where $H_i(y,z) > H_0$. Taking the tip-to-film-surface distance as $d = 100$ nm, and the film thickness $a = 20$ nm, a least-squares fit of the truncated parabola to the dipole field yields $C_0 = 0.41$, $C_z = 0.543/R^2$, and $C_y = 0.0942/R^2$. The constant C_z is more than five times larger than C_y, which means that the parabola is "'steeper" in the z direction than it is in the y direction.

To gauge the accuracy of the analytic results, we performed micromagnetic calculations of the spin-wave dynamics in the parabolic field wells. The images in Fig. 4 depict the lossy part of susceptibility of the magnetization as a function of field and frequency. The images are compiled from individual spectra that were obtained by Fourier transform of the ring-down

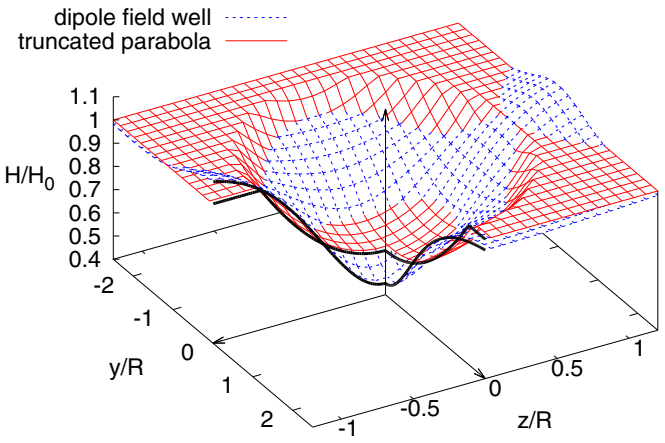

FIG. 3. The spatial dependence of the normalized dipolar field from the micromagnetic tip. Two-dimensional potential well, calculated by the formula $H_i/H_0 = f(y,z) - 1$, fitted by two-dimensional harmonic oscillator potential $-C_0 + C_z z^2 + C_y y^2$, where $C_0 = 0.41$, $C_z = 0.543/R^2$, $C_y = 0.0942/R^2$.

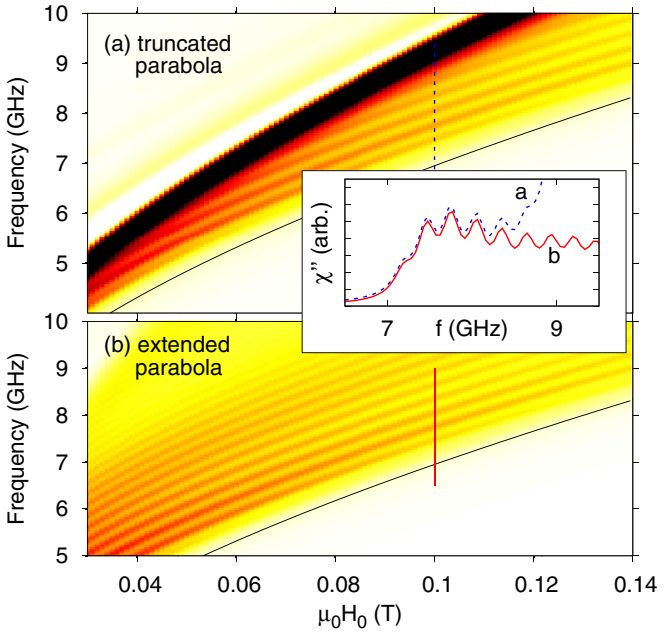

FIG. 4. Dispersion of spin-wave modes in parabolic field wells calculated by micromagnetic modeling as functions of applied field H_0. Material parameters are as follows: saturation magnetization of the film, $M_0 = 700$ kA/m; gyromagnetic ratio, $\gamma/2\pi = 29.6$ GHz/T; exchange stiffness, $A = 10^{-11}$ J/m; and film thickness $a = 20$ nm. The parameters of the parabolic well C_0, C_z, C_y approximate a dipole field (see text and Fig. 3). (a) Truncated parabolic well field profile. The dark band corresponds to resonance of the sheet film outside the well, while the lowest solid black line is the uniform-film precession frequency at the minimum field in the well, provided as a reference. (b) Resonances in an "infinite" parabolic well extending over the film plane. The inset shows spectra at 0.1 T for panels (a) and (b), respectively.

response to a field impulse. Figure 4(a) shows the frequencies of spin-wave modes for a truncated parabola approximation to the tip field (see Fig. 3). The thick dark band corresponds to precession in the region outside the field well. The lower solid line is a visual reference that shows the uniform-film precession frequency corresponding to the minimum field in the well, $H_0(1 - C_0)$.

For comparison, Fig. 4(b) shows the results calculated for an extended parabolic field acting over the whole film plane, using the same values for C_0, C_z, and C_y. The inset compares the imaginary part of the susceptibility at 0.1 T, and shows very similar behavior for the lowest modes in the full parabola and in the truncated parabola. For both types of field well, the trapped spin-wave modes appear as a series of resonances, roughly equally spaced, and roughly equal in amplitude except the lowest mode, which appears as a shoulder in the spectra. These features are also characteristics of previous experimental results for localized spin waves in a tangentially magnetized film [30]. Profiles of the lowest modes, calculated by micromagnetic modeling at $\mu_0 H_0 = 0.1$ T, are given in Fig. 5. We will discuss these profiles in comparing with analytical results below.

Now we return to the approach developed in Sec. II, and we compare the micromagnetic calculations with the results generated by the diagonal approximation. For convenience, we denominate a mode with the profile $\varphi_{mn}(\eta,\xi) = \psi_m(\eta)\psi_n(\xi)$ by a pair of corresponding indices (m,n), where the first index determines the y dependence, and the second index determines the z dependence of the mode's profile in the film plane.

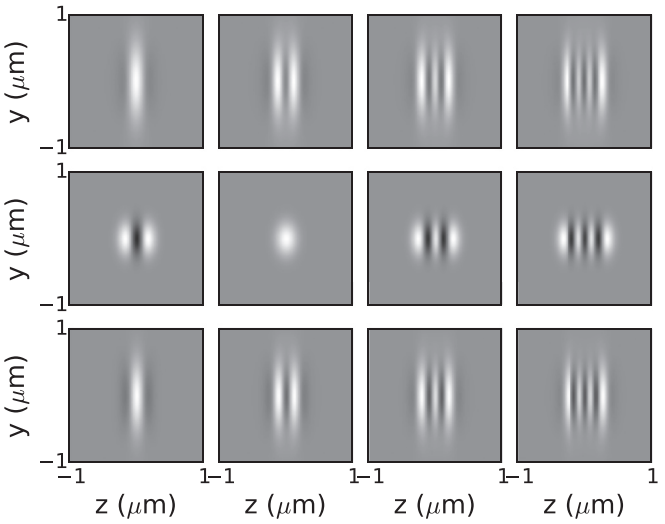

FIG. 5. Mode profiles of the localized excitations calculated with different approximations. The field and equilibrium magnetization lie along the z axis. Profiles are presented in order of increasing frequency. Top row: Profiles calculated by micromagnetic modeling at $\mu_0 H_0 = 0.1$ T, corresponding to the shoulder and the first three maxima in the inset of Fig. 4. Middle row: Mode profiles for the diagonal approximation, equivalent to Hermite function basis states $\varphi_{0,m}$ for $m = \{2,0,4,6\}$. With magnetostatic interactions, the (0,2) mode has a lower frequency than the (0,0) mode. Bottom row: Eigenmode profiles when hybridization via magnetostatic interactions is taken into account, showing strong similarities to the micromagnetic results.

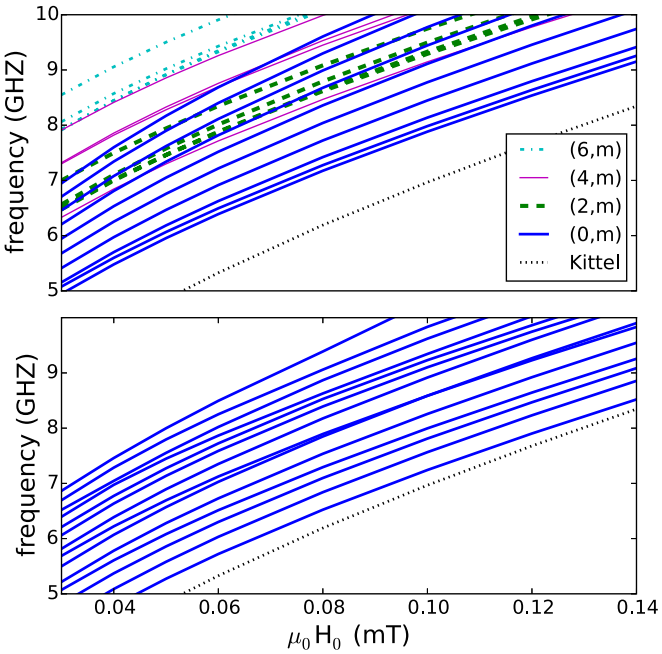

FIG. 6. Calculated dispersion of precession modes using (a) Hermite function mode profiles and a diagonal approximation and (b) when hybridization by magnetostatic interactions is taken into account. Similarly to Fig. 4, the lower black dotted lines correspond to the uniform precession frequency in the minimum field.

We consider only even indices, as only the modes with even symmetry can be excited by a uniform driving field.

Mode frequencies calculated in the diagonal approximation by Eq. (10), are presented in Fig. 6(a). The lowest part of the spectra consists of a branch of modes with indices $(0,n)$ which are localized analogs of backward volume waves with wavefronts perpendicular to the static magnetization and common y dependence $\exp(-\eta^2/2)$. Additionally, frequencies of a few modes from the $(2,n)$, $(4,n)$, and $(6,n)$ branches are plotted and these modes generally have higher frequencies than the $(0,n)$ branch.

For this example field well, the diagonal approximation yields results that are only qualitatively consistent with the micromagnetic solutions, and the diagonal approximation yields mode frequencies that are generally higher than the micromagnetic results. Note the gap between the lowest mode frequency and the dashed reference minimum-field line Fig. 6(a), and compare that with the much smaller corresponding gaps in Fig. 4. The mode frequencies are also less evenly spaced, especially for the lowest frequency modes. Interestingly, the lowest frequency mode is the (0,2) mode, not the (0,0) mode.

The mode profiles, which are identical to the basis state profiles, are shown in Fig. 5 (middle). These take the form of standing waves along the field direction, similar to the modes in the micromagnetic results in Fig. 5 (top). However, clear differences can be seen between the calculated micromagnetic profiles and the profiles of the Hermite functions with the same parabolic well parameters [Fig. 5 (middle)]. The most striking difference is that the micromagnetic mode profiles are extended further in the y direction. A subtler difference can be seen in the first profile in the top row. On either side of the central maximum, there are slight minima visible as weak, vertical dark streaks. The extension of the mode profiles in the y direction and the extra minima in the profiles relative to the basis profiles indicate that mode hybridization is needed to improve upon the diagonal approximation.

The failures of the diagonal approximation are perhaps not surprising. The validity criterion defined in the previous section, $\epsilon_i \equiv a/(DK_i) \ll 1$, is not well satisfied for this example. For the present example, $\epsilon_y = 1.0$ and $\epsilon_z = 0.7$. We can expect magnetostatic mode interactions to be important, and we explore these effects in the following section.

IV. BEYOND THE DIAGONAL APPROXIMATION

In the previous section we found that the diagonal approximation yields only a qualitative prediction compared to the micromagnetic results. Here we look for a full solution using the full set of Hermite function basis states while including magnetostatic interactions between those states.

First, we combine the two first-order equations of motion in (4) using substitution to obtain a single second-order equation of motion for m_x. Then we expand the excitations as a superposition of basis states

$$m_x \propto a_p(\eta,\xi) = \sum_{mn} A_{p,mn}\varphi_{mn}(\eta,\xi). \tag{15}$$

The equations of motion then become an infinite system of linear equations for coefficients A_{mn} coupled by the off-diagonal magnetostatic elements, $\langle h_x\rangle_{mn,m'n'}$ and $\langle h_y\rangle_{mn,m'n'}$. Calculation of these terms is described in the Appendices. We find that the off-diagonal coupling values generally weaken with "distance" from the diagonal, i.e., $|m-m'|$ and $|n-n'|$, and this fact allows us to approximate the full problem with a finite-sized subset of the basis states. By numerically diagonalizing the dynamical matrix, we obtain the eigenfrequencies Ω_p and the eigenmode profiles $a_p(\eta,\xi)$, and we choose the normalization of the profiles such that $\int |a_p(\eta,\xi)|^2 d\eta\, d\xi = 1$.

In the results we show below, we have limited the basis set to functions with even indices (m,n), where both n and m vary from 0 to 28. The choice of even indices addresses the case of a uniform excitation field where odd-symmetry modes would not be excited. Images of the 12 lowest-frequency eigenmodes are shown in Fig. 7 in order of increasing eigenfrequency. The first three modes (with numbers 0, 1, and 2) and the fourth, sixth, and ninth ones have profiles with vertical nodal lines similar to the micromagnetic images [Fig. 6 (top)]. However, a distinct set of modes appears (the third, the fifth, the seventh, the eighth and so on) with additional horizontal nodal lines. Resonances from this second set are not prominent in the micromagnetic results.

As an explanation for the apparent absence of certain modes from the micromagnetic results, we show next that these modes couple weakly to a uniform driving field. The intensity of each mode p with spatial profile $a_p(\eta,\xi)$ is calculated as

$$I_p = \frac{\left[\int dy\, dz\; a_p(K_y y, K_z z)\right]^2}{\int dy\, dz\; a_p(K_y y, K_z z)^2}. \tag{16}$$

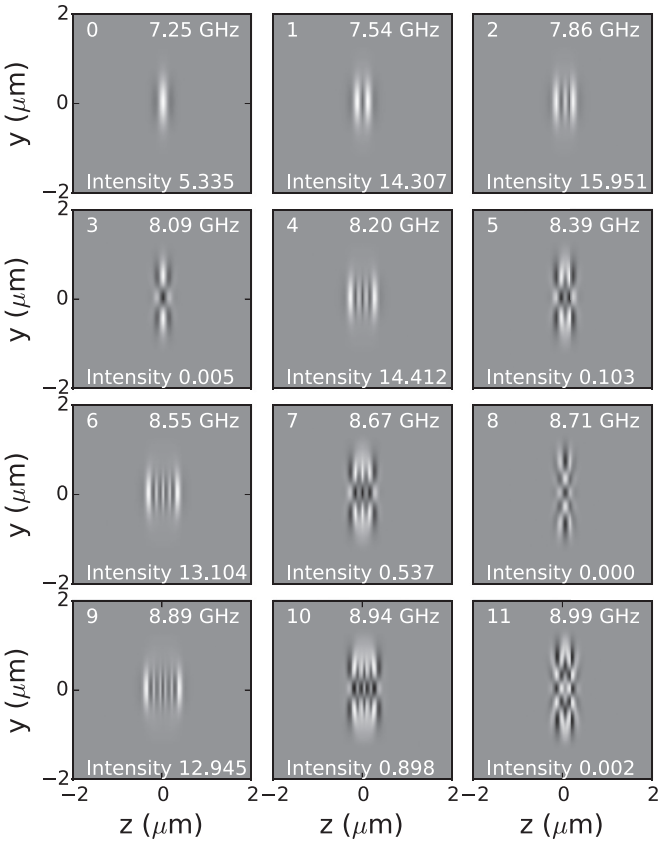

FIG. 7. Mode profiles of the 12 lowest modes, calculated on the basis of an array of functions $\varphi_{mn}(\eta,\xi)$ with even indices (m,n), where both m and n vary from 0 to 28. Corresponding frequencies (intensities) are given in the upper right (lower left) corners of every image. Magnetic parameters and parabolic well were defined in the previous section. Applied field $\mu_0 H_0 = 0.1$ T.

The integral in the numerator of this expression is proportional to the Zeeman interaction between the transverse magnetization in the mode and a uniform, transverse applied driving field. The integral is squared; in an absorption experiment, this coupling integral acts twice, once as the field excites the mode, and a second time as the precession acts on the field source. The intensity values for the modes are provided in each image in Fig. 7. Calculated intensities of the modes vs their frequencies are given in Fig. 8. The modes with largest intensities comprise a set of peaks roughly equally spaced in frequency and roughly equivalent intensity, in agreement with the micromagnetic spectra presented in Fig. 4. Profiles of these modes are very similar to the images in Fig. 5. The low intensity of the lowest frequency mode is also captured by the eigenmode calculation.

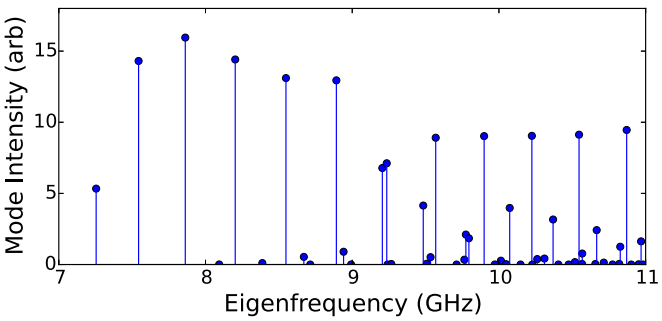

FIG. 8. Intensities vs frequencies for hybridized modes calculated on the basis of an array of functions $\varphi_{mn}(\eta,\xi)$ with even indices (m,n), where both m and n vary from 0 to 28. Intensities describe coupling to a uniform microwave field, as in ferromagnetic resonance experiments. Corresponding profiles for the lowest 12 modes were presented in Fig. 7.

V. DISCUSSION

Summarizing, we present here calculations of localized spin-wave modes that are excited in a parabolic field well. The model treats the field well and exchange interactions exactly by using Hermite functions as mode profiles. However, numerical computation was required to incorporate the magnetostatic interactions with sufficient fidelity to agree with results obtained by micromagnetic simulation.

For analysis of localized spin-wave modes, the selection of the basis functions is dictated by the symmetry of the situation [31]. For thin films in uniform fields, plane waves are the obvious basis choice due to translational invariance and the fact that the plane waves are also eigenfunctions of the applied field, exchange, and magnetostatic interactions [29]. In confined structures, the plane waves are no longer eigenfunctions of the magnetostatic interactions or of possible nonuniform static internal fields, but plane waves remain a good choice for analysis of excitations in rectangular dots [32] and in stripes [33].

For a normally magnetized film, the axial symmetry suggests the use of Bessel functions. In the case of a field well with axial symmetry, the field breaks the radial uniformity, and the Bessel function profiles are no longer eigenfunctions of the applied field. Also, the precession contains in-plane components of magnetization that break the axial symmetry, and the Bessel function field profile is not an eigenfunction of the in-plane magnetostatic interactions. Despite these shortcomings, Bessel-function basis functions have been used to good effect in circular dots [22,28,34], and in normally magnetized field wells [21,23–25].

Symmetry is not the driving motivation for using Hermite functions in the tangentially magnetized field well case. Rather the motivation comes from the Hermite functions' ability to solve the combination of the parabolic field well profile and the exchange interaction. Improving solutions are then found with increasingly sophisticated approximations to the magnetostatic interactions between a modest number of basis states. The use of Hermite functions also simplifies the calculation of magnetostatic interactions by virtue of the fact that they are essentially their own Fourier transforms.

In closing we note that the method we have used here is not limited to the in-plane case. The method can be easily generalized for different orientations of the applied field relative to the film plane, and it may prove to be useful in planning future ferromagnetic resonance imaging experiments involving spin wave localization [24]. In particular, the method is applicable to the case of normally magnetized film [21], when the potential well is either isotropic or anisotropic.

ACKNOWLEDGMENTS

One of the authors (E.V.T.) appreciates the Fulbright Program in Ukraine for the financial support of this work. She is grateful to colleagues at NIST, Julie Borchers, Brian Kirby, Kathryn Krycka, and Alex Grutter for fruitful discussions and hospitality.

APPENDIX A: CALCULATION OF MAGNETOSTATIC INTERACTIONS

In general, magnetization precession produces dynamic fields that then exert torques on the magnetization. In this appendix, we describe the magnetostatic coupling that occurs when the field produced in one mode, (m,n), acts on a mode (m',n'). Equation (12) describes the case when $(m,n) = (m',n')$, but here we treat the more general case of interaction between possibly different modes. The magnetostatic interaction terms are given by

$$\langle h_i\rangle_{mn,m'n'} = -\frac{M_0 K_y K_z}{4\pi a}\int d\mathbf{r}\int d\mathbf{r}'\varphi_{mn}(\eta,\xi,)\,\varphi_{m'n'}(\eta',\xi') \times \frac{\partial}{\partial i}\frac{\partial}{\partial i'}\frac{1}{|\mathbf{r}-\mathbf{r}'|}, \tag{A1}$$

where i stands for x or y and the dimensionless coordinates are $\xi = K_z z$, $\eta = K_y y$.

To simplify the sixfold integral in (A1) we use Fourier transforms of the integrand terms. The reward is gained from the fact that the nonlocal kernel of the integral in (12) becomes a local function in reciprocal space. In terms of Fourier transform, the kernel can be expressed as

$$\frac{1}{|\mathbf{r}-\mathbf{r}'|} = \int \frac{d\mathbf{q}}{(2\pi)^2}\frac{2\pi}{q}e^{-q|x-x'|}e^{i\mathbf{q}(\rho-\rho')}, \tag{A2}$$

where ρ and ρ' are two-dimensional vectors (y,z) and (y',z'), correspondingly.

The remaining in-plane integrals over y, y', z, and z' are simplified by using the Fourier transform of the Hermite functions (6). Here the Hermite functions yield an additional unique advantage: their Fourier transforms are proportional to the functions themselves.

$$\psi_n(x) = \frac{1}{(i)^n\sqrt{2\pi}}\int_{-\infty}^{\infty} dk\,\psi_n(k)e^{ikx}. \tag{A3}$$

As a result, the magnetostatic matrix elements (12) simplify to twofold integrals

$$\langle h_x\rangle_{mn,m'n'} \approx -M_0\iint du\,dv\frac{[1-e^{-qa}]}{qa}\varphi_{mn}(u,v)\varphi_{m'n'}(u,v), \tag{A4a}$$

$$\langle h_y\rangle_{mn,m'n'} \approx -M_0\iint du\,dv\,\frac{q_y^2}{q^2}\left\{1-\frac{1-e^{-qa}}{qa}\right\} \times \varphi_{mn}(u,v)\,\varphi_{m'n'}(u,v), \tag{A4b}$$

where $\varphi_{mn}(u,v)$ are the mode profiles given by (6)–(9), $\mathbf{q} = (q_y,q_z) = (K_y u, K_z v)$, and $q = \sqrt{(K_y u)^2 + (K_z v)^2}$.

APPENDIX B: MAGNETOSTATIC INTERACTIONS IN THE THIN FILM LIMIT

In the thin film limit, the coefficients given by (A4) can be approximated by a first-order expansion in $aK_i \ll 1$. Because the functions $\psi_n(u)$ decay strongly as $\exp(-u^2/2)$ we can use an expansion in aq under the integrals. Then we obtain the diagonal matrix elements of a dipole-dipole operator in a linear approximation.

$$\langle h_y\rangle_{mn,m'n'} = -M_0 a K_y Y_{mn}, \tag{B1a}$$

$$\langle h_x\rangle_{mn,m'n'} = -M_0(1 - aK_y X_{mn}), \tag{B1b}$$

$$X_{mn,m'n'} = \iint du\,dv\,\frac{q}{2K_y}\varphi_{mn}(u,v)\,\varphi_{m'n'}(u,v), \tag{B2a}$$

$$Y_{mn,m'n'} = \iint du\,dv\,\frac{q_y^2}{2K_y q}\varphi_{mn}(u,v)\,\varphi_{m'n'}(u,v). \tag{B2b}$$

TABLE I. Numerical values of X_{0n} and Y_{0n} depending on $C = \sqrt{C_z/C_y}$.

C	X_{00}	Y_{00}	X_{02}	Y_{02}	X_{04}	Y_{04}	X_{06}	Y_{06}	X_{08}	Y_{08}
0	0.282	0.282	0.282	0.282	0.282	0.282	0.282	0.282	0.282	0.282
0.2	0.332	0.256	0.482	0.211	0.552	0.19	0.627	0.176	0.692	0.166
0.4	0.366	0.244	0.571	0.187	0.707	0.164	0.818	0.149	0.915	0.139
0.6	0.395	0.235	0.659	0.172	0.831	0.148	0.97	0.134	1.091	0.124
0.8	0.42	0.228	0.735	0.161	0.937	0.137	1.101	0.124	1.242	0.114
1.0	0.443	0.222	0.803	0.152	1.032	0.129	1.216	0.116	1.375	0.107
1.2	0.465	0.216	0.866	0.146	1.119	0.123	1.322	0.11	1.497	0.101
1.4	0.485	0.212	0.923	0.14	1.199	0.117	1.419	0.104	1.609	0.096
1.6	0.504	0.208	0.978	0.135	1.273	0.113	1.51	0.1	1.713	0.092
1.8	0.522	0.204	1.029	0.131	1.344	0.109	1.595	0.097	1.812	0.088
2.0	0.539	0.201	1.178	0.127	1.411	0.106	1.677	0.093	1.905	0.085
2.2	0.555	0.198	1.124	0.124	1.475	0.102	1.754	0.091	1.994	0.083
2.4	0.571	0.195	1.169	0.121	1.536	0.1	1.828	0.088	2.079	0.08
2.6	0.587	0.192	1.211	0.119	1.594	0.097	1.899	0.086	2.161	0.078
2.8	0.602	0.19	1.253	0.116	1.851	0.095	1.968	0.084	2.239	0.076
3.0	0.616	0.188	1.293	0.114	1.705	0.093	2.034	0.082	2.315	0.074

Numerical coefficients X and Y depend only on the ratio of curvature parameters, $\sqrt{C_z/C_y}$.
In those cases where diagonal approximation is expected to be valid and where the thin film limit holds, a good description of the trapped modes can be obtained using a few magnetostatic matrix elements from the diagonal. The lowest branch values of X_{0n} and Y_{0n} will give magnetostatic corrections to the exchange-dominated frequencies. These values for different values of $C = \sqrt{C_z/C_y}$ are presented in Table I.

[1] S. O. Demokritov and B. Hillebrands, *Spinwaves in Laterally Confined Magnetic Structures*, Topics in Applied Physics Vol. 83 (Springer-Verlag, Berlin, Heidelberg, 2002), pp. 65–92.
[2] J. W. Lau and J. M. Shaw, J. Phys. D **44** (2011).
[3] R. D. McMichael, D. J. Twisselmann, and A. Kunz, Phys. Rev. Lett. **90**, 227601 (2003).
[4] J. P. Park, P. Eames, D. M. Engebretson, J. Berezovsky, and P. A. Crowell, Phys. Rev. Lett. **89**, 277201 (2002).
[5] J. Jorzick, S. O. Demokritov, B. Hillebrands, M. Bailleul, C. Fermon, K. Y. Guslienko, A. N. Slavin, D. V. Berkov, and N. L. Gorn, Phys. Rev. Lett. **88**, 047204 (2002).
[6] R. D. McMichael and B. B. Maranville, Phys. Rev. B **74**, 024424 (2006).
[7] V. V. Kruglyak, A. Barman, R. J. Hicken, J. R. Childress, and J. A. Katine, Phys. Rev. B **71**, 220409 (2005).
[8] V. V. Kruglyak, P. S. Keatley, R. J. Hicken, J. R. Childress, and J. A. Katine, J. Appl. Phys. **99**, 08F306 (2006).
[9] B. B. Maranville, R. D. McMichael, and D. W. Abraham, Appl. Phys. Lett. **90**, 232504 (2007).
[10] M. Zhu and R. D. McMichael, J. Appl. Phys. **107**, 103908 (2010).
[11] M. Zhu and R. D. McMichael, J. Appl. Phys. **109**, 043904 (2011).
[12] H. T. Nembach, J. M. Shaw, T. J. Silva, W. L. Johnson, S. A. Kim, R. D. McMichael, and P. Kabos, Phys. Rev. B **83**, 094427 (2011).
[13] F. Guo, L. M. Belova, and R. D. McMichael, Phys. Rev. Lett. **110**, 017601 (2013).
[14] A. Slavin and V. Tiberkevich, Phys. Rev. Lett. **95**, 237201 (2005).
[15] S. Bonetti, V. Tiberkevich, G. Consolo, G. Finocchio, P. Muduli, F. Mancoff, A. Slavin, and J. Åkerman, Phys. Rev. Lett. **105**, 217204 (2010).
[16] R. H. Liu, W. L. Lim, and S. Urazhdin, Phys. Rev. Lett. **110**, 147601 (2013).
[17] S. M. Mohseni, S. R. Sani, J. Persson, T. N. A. Nguyen, S. Chung, Y. Pogoryelov, P. K. Muduli, E. Iacocca, A. Eklund, R. K. Dumas *et al.*, Science **339**, 1295 (2013).
[18] E. Iacocca, R. K. Dumas, L. Bookman, M. Mohseni, S. Chung, M. A. Hoefer, and J. Åkerman, Phys. Rev. Lett. **112**, 047201 (2014).
[19] M. D. Maiden, L. D. Bookman, and M. A. Hoefer, Phys. Rev. B **89**, 180409 (2014).
[20] S. O. Demokritov and A. N. Slavin, *Handbook of Magnetism and Advanced Magnetic Materials* (Wiley, New York, 2007).
[21] I. Lee, Y. Obukhov, G. Xiang, A. Hauser, F. Yang, P. Banerjee, D. Pelekhov, and P. Hammel, Nature (London) **466**, 845 (2010).
[22] G. N. Kakazei, P. E. Wigen, K. Y. Guslienko, V. Novosad, A. Slavin, V. Golub, N. A. Lesnik, and Y. Otani, Appl. Phys. Lett. **85**, 443 (2004).
[23] R. Adur, C. Du, H. Wang, S. A. Manuilov, V. P. Bhallamudi, C. Zhang, D. V. Pelekhov, F. Yang, and P. C. Hammel, Phys. Rev. Lett. **113**, 176601 (2014).
[24] C. Du, R. Adur, H. Wang, S. A. Manuilov, F. Yang, D. V. Pelekhov, and P. C. Hammel, Phys. Rev. B **90**, 214428 (2014).
[25] R. Adur, C. Du, S. A. Manuilov, H. Wang, F. Yang, D. V. Pelekhov, and P. C. Hammel, J. Appl. Phys. **117**, 17E108 (2015).
[26] E. Nazaretski, D. V. Pelekhov, I. Martin, M. Zalalutdinov, D. Ponarin, A. Smirnov, P. C. Hammel, and R. Movshovich, Phys. Rev. B **79**, 132401 (2009).
[27] B. Kalinikos, N. Kovshikov, P. Kolodin, and I. Panchurin, Elektronnaya Tehnika Ser. Elektronika SVCH **382**, 53 (1985).
[28] K. Y. Guslienko and A. Slavin, J. Appl. Phys. **87**, 6337 (2000).
[29] B. A. Kalinikos and A. N. Slavin, J. Phys. C **19**, 7013 (1986).
[30] H.-J. Chia, F. Guo, L. M. Belova, and R. D. McMichael, Phys. Rev. Lett. **108**, 087206 (2012).
[31] M. Pardavi-Horvath and E. Tartakovskaya, *Magnetic Nano- and Microwires. Design, Synthesis, Properties and Applications*, edited by M. Vazques, Woodhead Publishing Series in Electronic and Optical Materials (Woodhead Publishing, Amsterdam, 2015), Chap. 23.
[32] C. Bayer, J. Jorzick, B. Hillebrands, S. O. Demokritov, R. Kouba, R. Bozinoski, A. N. Slavin, K. Y. Guslienko, D. V. Berkov, N. L. Gorn *et al.*, Phys. Rev. B **72**, 064427 (2005).
[33] K. L. Livesey, J. Ding, N. R. Anderson, R. E. Camley, A. O. Adeyeye, M. P. Kostylev, and S. Samarin, Phys. Rev. B **87**, 064424 (2013).
[34] T. Mewes, J. Kim, D. V. Pelekhov, G. N. Kakazei, P. E. Wigen, S. Batra, and P. C. Hammel, Phys. Rev. B **74**, 144424 (2006).